Optimal Circle-to-Rectilinear Orbit Transfer with Circumferential Thrust

Alessandro A. Quarta*, Giovanni Mengali, Andrea Caruso

Department of Civil and Industrial Engineering, University of Pisa, I-56122 Pisa, Italy

Abstract

This paper investigates the optimal transfer trajectories from a circular parking orbit towards the apocenter of a rectilinear ellipse, where the spacecraft reaches a quasi-stationary condition relative to an inertial reference frame. The spacecraft is equipped with a propulsion system that provides a circumferential continuous propulsive acceleration, that is, an acceleration whose direction is perpendicular to the primary body-spacecraft line. The performance index to minimize is the total flight time, and an indirect method is used to analyze the transfer trajectories. In this context, the optimal transfer performance is obtained as a function of the spacecraft propulsive acceleration magnitude through an interpolation procedure of numerical simulations. The results obtained with a continuous thrust propulsion system are also compared with those derived from a multi-impulse transfer. Finally, the paper investigates a heliocentric mission scenario in which the spacecraft minimizes the flight time required to reach a rectilinear ellipse with a given value of the aphelion radius.

Keywords: Circumferential propulsive acceleration, rectilinear ellipse, optimal transfer, preliminary mission analysis, quasi-stationary condition

Nomenclature

$\boldsymbol{a}$	=	propulsive acceleration vector ($\mathrm{mm/s^2}$)
a_T	=	maximum propulsive acceleration magnitude ($\mathrm{mm/s^2}$)
c	=	scalar parameter
$\mathcal{H}$	=	Hamiltonian function
h	=	specific angular momentum ($\mathrm{km^2/s}$)
$\hat{\boldsymbol{\imath}}_r$	=	radial unit vector
$\hat{\boldsymbol{\imath}}_\theta$	=	circumferential unit vector
J	=	performance index
N	=	number of impulsive manoeuvres
r	=	radial distance (km)
$\boldsymbol{r}$	=	position vector (km)
$\mathcal{T}(O; r\,\theta)$	=	polar reference frame
T_0	=	parking orbit period (days)
t	=	time (s)
u	=	radial component of the spacecraft velocity (km/s)
v	=	circumferential component of the spacecraft velocity (km/s)
$\boldsymbol{v}$	=	velocity vector (km/s)

*Corresponding author

Email addresses: a.quarta@ing.unipi.it (Alessandro A. Quarta), g.mengali@ing.unipi.it (Giovanni Mengali), andrea.caruso@ing.unipi.it (Andrea Caruso)

Published in Astrodynamics, Vol. 3, No. 1, March 2019, pp. 31–43. doi: https://doi.org/10.1007/s42064-018-0034-9

Δt	=	time interval (s)
$\Delta \boldsymbol{v}$	=	velocity change vector (km/s)
θ	=	polar angle
λ_r, λ_u, λ_h	=	adjoint variables
μ	=	primary body gravitational parameter ($\mathrm{km}^3/\mathrm{s}^2$)
τ	=	control parameter

Subscripts

0	=	initial time
A	=	apocenter
e	=	end of a leg
f	=	final time
I	=	switching point
imp	=	multi-impulse case
int	=	interval
s	=	beginning of a leg
tot	=	total
$\odot$	=	Sun

Superscripts

$\star$	=	optimal value
$\sim$	=	dimensionless parameter
$\cdot$	=	time derivative
$'$	=	derivative with respect to $\widetilde{t}$

1. Introduction

The spacecraft trajectory generated by a constant, continuous, propulsive acceleration with a fixed direction relative to an orbital reference frame is a classical astrodynamics problem [1, 2], which offers interesting analytical results useful for a preliminary mission design [3]. For mathematical tractability, the spacecraft motion under a constant and continuous thrust is often addressed in some noteworthy situations, including the purely radial, tangential or circumferential cases. The latter scenario in which the propulsive acceleration direction is always orthogonal to the primary body-spacecraft line, has been recently studied by Niccolai et al. [4] from a viewpoint substantially different than that adopted by the classical works by Tsien [1] or Battin [2]. In particular, the equations of motion have been written with the aid of non-singular orbital parameters, using the perturbative analysis originally proposed by Bombardelli et al. [5]. That way, the spacecraft propelled trajectory is described in analytic form under the assumptions of a circle-to-circle orbit raising (or lowering) and a small propulsive acceleration when compared to the local gravitational pull.

Escape trajectories from a circular parking orbit are exemplary trajectories that may be attained using a constant circumferential propulsive acceleration. In particular, the minimum time necessary to reach the escape conditions from the gravitational attraction of a primary body may be obtained, in an analytical form , by suitably simplifying the spacecraft equations of motion [1, 2], or through analytical relations interpolating the results from numerical simulations [6]. Other mission applications with a constant circumferential thrust are possible and, indeed, this paper concentrates on the possibility of reaching the apocenter of an Elliptic Rectilinear Orbit (ERO).

An ERO is an elliptic Keplerian orbit whose pericenter distance tends to zero and, as such, the ellipse degenerates into a line segment connecting the primary body center-of-mass to the ERO apocenter [7]. It is characterized by a circumferential component of the orbital velocity vector equal to zero. In the neighborhood of the apocenter the orbital velocity is close to zero (since even the radial velocity component tends to zero) and so the spacecraft experiences a near-heliostationary condition that would be otherwise impossible to obtain with other trajectory types. Possible scientific applications related to the achievement

of a heliostationary condition are discussed at length in a paper by Dandouras et al. [8], where the use of a propellantless propulsion system (an ideal solar sail) is first proposed for such an advanced mission concept. This same mission scenario has been later studied with more accurate models of the thrust vector characteristics. In particular, the optimal performance of a non-ideal solar sail in a mission towards a heliostationary condition have been calculated in Ref. [9], while Refs. [10, 11] propose the concept of a mission towards an ERO to reach a near-heliostationary condition in the apocenter zone. The main feature of an ERO is that the spacecraft is able to track a descent rectilinear trajectory toward the attracting body, whose interesting scientific consequences are thoroughly discussed by Colombo e al. [12].

This paper focuses on the minimum time trajectories necessary to transfer a spacecraft from a circular parking orbit of given radius to the apocenter of an ERO. The results are expressed as a function of the maximum magnitude of the circumferential propulsive acceleration. The problem is studied assuming a two-dimensional mission case in which the distance between the ERO apocenter and the primary center of mass is not given a priori, but is an output of the optimization process. The optimal trajectories are calculated using an indirect approach and, in this context, the paper (graphically) reports the initial values of the adjoint variables as a function of the propulsion system characteristics. These values are necessary to solve the two-point boundary value problem associated to the optimum problem, and to simulate the minimum-time trajectory. In particular, the optimal control law is shown to be particularly simple to manage, as there exists a single point only where the thrust vector reverses its direction with respect to an orbital reference frame. The same mission scenario has also been studied assuming an optimal multi-impulse transfer with a direct approach and, in this case, the simulation results have both confirmed the optimality of the trajectories obtained with a continuous thrust and revealed the optimal multi-impulse strategy.

The paper is organized as follows. The next section discusses the mathematical model used to calculate the minimum-time trajectories from a circular orbit to an ERO whose apocenter distance is unconstrained. The mathematical model is then used in a parametric study of the optimal performance as a function of the (maximum) propulsive acceleration magnitude. The numerical results obtained with a continuous thrust are compared to those achievable with an optimal multi-impulse transfer strategy. Finally, the last section contains some concluding remarks.

2. Mathematical Model

Assume a spacecraft to be initially placed on a circular parking orbit with radius r_0 around a primary body with gravitational parameter μ. Introduce a polar reference frame $\mathcal{T}(O; r\,\theta)$ with its origin in the primary center of mass, while $\hat{\boldsymbol{i}}_r$ and $\hat{\boldsymbol{i}}_\theta$ are the radial and circumferential unit vectors, respectively. The primary propulsion system provides a purely circumferential acceleration $\boldsymbol{a}$ (that is, a propulsive acceleration whose direction is orthogonal to the primary-spacecraft line, see Fig. 1), given by

$$\boldsymbol{a} = \tau\, a_T\, \hat{\boldsymbol{i}}_\theta \tag{1}$$

where a_T is the maximum acceleration magnitude, and τ, which models the thrust level, is a dimensionless control variable that may be varied with continuity within the interval $[-1,\, 1]$, with $\tau \gtrless 0$ according to whether $\boldsymbol{a} \cdot \hat{\boldsymbol{i}}_\theta \gtrless 0$. The spacecraft equations of motion in $\mathcal{T}$ are:

$$\dot{r} = u \tag{2}$$

$$\dot{\theta} = \frac{h}{r^2} \tag{3}$$

$$\dot{u} = -\frac{\mu}{r^2} + \frac{h^2}{r^3} \tag{4}$$

$$\dot{h} = \tau\, r\, a_T \tag{5}$$

where r is the primary-spacecraft distance, $|h|$ is the magnitude of the spacecraft specific angular momentum, u is the radial component of the spacecraft velocity (note that the circumferential component of the spacecraft velocity is $v = h/r$), and θ is the polar angle measured counterclockwise from the primary body-spacecraft

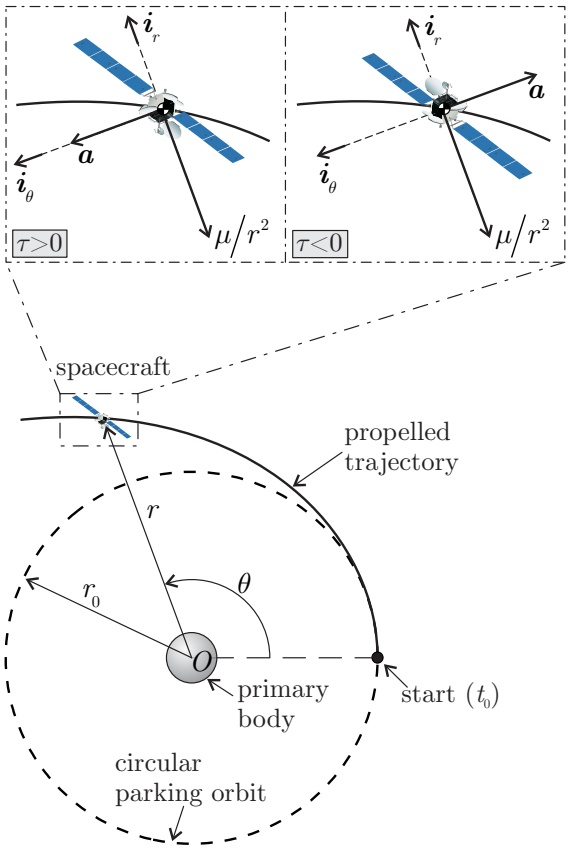

Figure 1: Reference frame and transverse propulsive acceleration concept.

line at the initial time $t_0 \triangleq 0$, that is, when the propulsion system is switched-on. The boundary conditions for a circular orbit are

$$r(t_0) = r_0 \quad , \quad \theta(t_0) = 0 \quad , \quad u(t_0) = 0 \quad , \quad h(t_0) = \sqrt{\mu\, r_0} \tag{6}$$

where $\theta(t_0)$ is assumed to be zero without loss of generality, see Fig. 1.

In the absence of any constraint on the spacecraft angular position and assuming τ to be independent of θ, the time variation of the osculating orbit characteristics may be studied through Eqs. (2), (4) and (5) only. To that end, introduce the dimensionless variables

$$\widetilde{r} \triangleq \frac{r}{r_0} \quad , \quad \widetilde{u} \triangleq \frac{u}{\sqrt{\mu/r_0}} \quad , \quad \widetilde{h} \triangleq \frac{h}{\sqrt{\mu\, r_0}} \quad , \quad \widetilde{a}_T \triangleq \frac{a_T}{\mu/r_0^2} \quad , \quad \widetilde{t} \triangleq \frac{t}{\sqrt{r_0^3/\mu}} \tag{7}$$

Using the prime symbol to denote a derivative taken with respect to $\widetilde{t}$, the dimensionless equations of motion become

$$\widetilde{r}' = \widetilde{u} \quad , \quad \widetilde{u}' = -\frac{1}{\widetilde{r}^2} + \frac{\widetilde{h}^2}{\widetilde{r}^3} \quad , \quad \widetilde{h}' = \tau\, \widetilde{r}\, \widetilde{a}_T \tag{8}$$

with initial conditions

$$\widetilde{r}(\widetilde{t}_0) = \widetilde{h}(\widetilde{t}_0) = 1 \quad , \quad \widetilde{u}(\widetilde{t}_0) = 0 \tag{9}$$

Note that when the maximum thrust level $\widetilde{a}_T$ and the control law $\tau = \tau(\widetilde{t})$ are given, Eqs. (8) and (9) allow the spacecraft dynamics to be simulated independent of the parking orbit radius r_0 and the primary gravitational parameter μ.

2.1. Trajectory optimization

For a given value of the maximum propulsive acceleration magnitude a_T (or $\widetilde{a}_T$), the problem is to find the minimum time interval $\Delta t = t_f - t_0 \equiv t_f$ necessary for the spacecraft to reach the apocenter A of an ERO. The distance from A to the primary's center of mass is not assigned, but is obtained as an output of the optimization process. In correspondence of point A, the spacecraft is at a stationary condition relative to the primary, since its inertial velocity is equal to zero. When the spacecraft is in the proximity of the apocenter, it therefore experiences a near-heliostationary condition of great scientific interest for space observation, especially when the primary body is the Sun, as is discussed in Refs. [8, 13, 14].

The minimum-time problem is mathematically equivalent to finding the time history of the control variable $\tau^\star = \tau(t)$ (or $\tau^\star = \tau(\widetilde{t})$), which maximizes the scalar performance index

$$J \triangleq -t_f \tag{10}$$

with the final boundary conditions

$$u(t_f) = 0 \quad , \quad h(t_f) = 0 \tag{11}$$

Since Eqs. (11) do not involve the angular coordinate θ, the minimum transfer time may be calculated with the dimensionless relations (8). Likewise, Eqs. (11) are replaced by their dimensionless counterpart

$$\widetilde{u}(\widetilde{t}_f) = 0 \quad , \quad \widetilde{h}(\widetilde{t}_f) = 0 \tag{12}$$

where $\widetilde{t}_f = t_f/\sqrt{r_0^3/\mu}$ is the final dimensionless time. The problem is addressed with an indirect approach [15, 16] by introducing the Hamiltonian function

$$\mathcal{H} \triangleq \lambda_r\, \widetilde{u} + \frac{\lambda_u}{\widetilde{r}^2}\left(\frac{\widetilde{h}^2}{\widetilde{r}} - 1\right) + \lambda_h\, \tau\, \widetilde{r}\, \widetilde{a}_T \tag{13}$$

where $\{\lambda_r,\, \lambda_u,\, \lambda_h\}$ are the dimensionless functions adjoint to $\{\widetilde{r},\, \widetilde{u},\, \widetilde{h}\}$. Their time derivatives are given by the Euler-Lagrange equations

$$\dot{\lambda}_r = -\frac{\mathrm{d}\mathcal{H}}{\mathrm{d}\widetilde{r}} = \frac{\lambda_u}{\widetilde{r}^3}\left(\frac{3\,\widetilde{h}^2}{\widetilde{r}} - 2\right) - \lambda_h\, \tau\, \widetilde{a}_T \tag{14}$$

$$\dot{\lambda}_u = -\frac{\mathrm{d}\mathcal{H}}{\mathrm{d}\widetilde{u}} = -\lambda_r \tag{15}$$

$$\dot{\lambda}_h = -\frac{\mathrm{d}\mathcal{H}}{\mathrm{d}\widetilde{h}} = -\frac{2\,\lambda_u\,\widetilde{h}}{\widetilde{r}^3} \tag{16}$$

with boundary conditions

$$\lambda_r(\widetilde{t}_f) = 0 \quad , \quad \mathcal{H}(\widetilde{t}_f) = 1 \tag{17}$$

Since $\mathcal{H}$ is a linear function of τ, see Eq. (13), from the Pontryagin's maximum principle the optimal control law $\tau^\star = \tau(\widetilde{t})$ is in the form of a bang-bang control, that is

$$\tau^\star = \mathrm{sign}\,(\lambda_h) \tag{18}$$

where $\mathrm{sign}\,(\square)$ is the signum function.

To summarize, for a given value of $\widetilde{a}_T$, the minimum flight time $\widetilde{t}_f$ is obtained by solving a Two-Point Boundary Value Problem (TPBVP) in which the unknowns $\{\lambda_r(\widetilde{t}_0),\, \lambda_u(\widetilde{t}_0),\, \lambda_h(\widetilde{t}_0),\, \widetilde{t}_f\}$ are calculated by enforcing the constraints given by Eqs. (12) and (17). The problem solution may be slightly simplified by noting that Eq. (13) does not depend explicitly on time and, as such, $\mathcal{H}$ is a constant of motion [15], that is, $\mathcal{H}(\widetilde{t}_0) = \mathcal{H}(\widetilde{t}_f) = 1$, see Eq. (17). When Eqs. (9) are substituted into (13) and the optimal control law (18) is suitably taken into account, the Hamiltonian function reduces to

$$\left|\lambda_h(\widetilde{t}_0)\right|\, \widetilde{a}_T = 1 \tag{19}$$

or

$$\lambda_h(\widetilde{t}_0) = \frac{\text{sign}\left(\lambda_h(\widetilde{t}_0)\right)}{\widetilde{a}_T} \tag{20}$$

with $\widetilde{a}_T \neq 0$. In other terms, sign $\left(\lambda_h(\widetilde{t}_0)\right) \in \{-1, 1\}$ is the new unknown to be found in place of $\lambda_h(\widetilde{t}_0)$. The TPBVP has been solved by means of a hybrid numerical technique that uses global optimization techniques to obtain a first guess of the adjoint variables, while the solution is then refined with gradient-based and direct methods [17]. In practice, a numerical continuation procedure, parameterized with the propulsive acceleration magnitude, has been used to reduce the computational effort in obtaining an estimate of the initial adjoint variables. Finally, Eqs. (8) have been integrated in double precision using a variable order Adams-Bashforth-Moulton solver scheme [18, 19] with absolute and relative errors of 10^{-12}.

3. Numerical simulations

The optimal transfer trajectories towards the apocenter of an ERO have been simulated with the previous mathematical model assuming $\widetilde{a}_T = \{0.01, 0.1, 1\}$. These three values of propulsive acceleration may be considered as representative of a propulsion system with a low, medium and high performance, respectively. In fact, $\widetilde{a}_T = 1$ corresponds to a maximum propulsive acceleration equal to the gravitational acceleration on the circular parking orbit, see Eqs. (7). For example, taking the Sun as the primary body and $r_0 = 1\,\text{au}$, $\widetilde{a}_T = 1$ implies $a_T \simeq 5.93\,\text{mm/s}^2$, which corresponds to a value well beyond the state-of-the-art performance of continuous-thrust propulsion systems.

The time histories of the spacecraft state variables $\{\widetilde{r}, \widetilde{u}, \widetilde{h}\}$ along the optimal transfer are shown in Fig. 2. As expected, the transfer times are strongly dependent on the propulsive acceleration magnitude and, indeed, they vary from $\widetilde{t}_f \simeq 100$ when $\widetilde{a}_T = 0.01$, see Fig. 2(a), to $\widetilde{t}_f \simeq 1.6$ when $\widetilde{a}_T = 1$, see Fig. 2(c). Recall that the dimensionless value of the parking orbit period is $\widetilde{T}_0 = 2\,\pi$. There is also a substantial variation of the apocenter distance $\widetilde{r}_A \triangleq \widetilde{r}(\widetilde{t}_f)$ from the primary, which decreases from $\widetilde{r}_A \simeq 10.5$ when $\widetilde{a}_T = 0.01$, to $\widetilde{r}_A \simeq 1.3$ when $\widetilde{a}_T = 1$. Figure 2 shows that the optimal trajectory towards the ERO

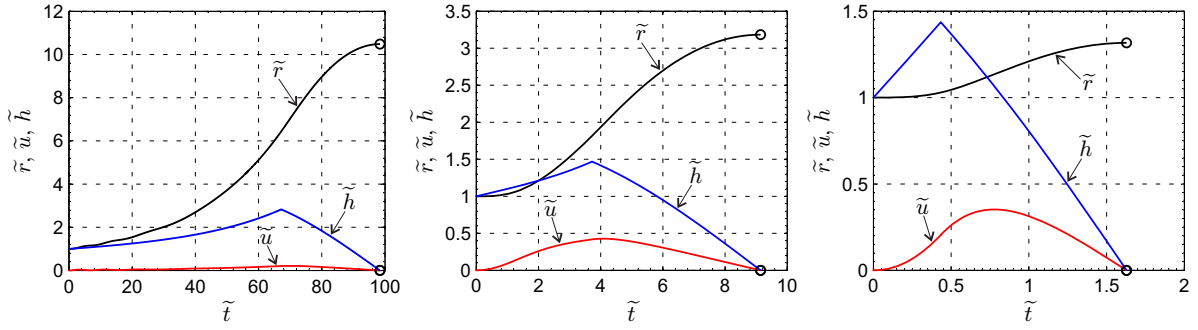

(a) $\widetilde{a}_T = 0.01$. (b) $\widetilde{a}_T = 0.1$. (c) $\widetilde{a}_T = 1$.

Figure 2: Time variation of dimensionless state variables $\{\widetilde{r}, \widetilde{u}, \widetilde{h}\}$ on the optimal trajectory.

apocenter may be divided into two parts. In a first phase the propulsive acceleration has a positive projection along $\hat{\boldsymbol{i}}_\theta$ ($\tau^\star = 1$), which increases the spacecraft angular momentum ($\widetilde{h}' > 0$). In a second phase, instead, $\boldsymbol{a} \cdot \hat{\boldsymbol{i}}_\theta < 0$ ($\tau^\star = -1$), thus inducing a progressive reduction of $\widetilde{h}$ until the final conditions of Eqs. (12) are met. Such a somewhat counterintuitive behavior of the optimal control law is clearly shown in Fig. 3, which illustrates the time history of $\tau^\star$ for the three values of $\widetilde{a}_T$. Other simulations, not reported in the paper, confirm that an initial phase with $\widetilde{h}' > 0$ exists for all values of $\widetilde{a}_T$ ranging in the interval $[0.01, 1]$. The latter remark allows the initial value of λ_h to be immediately found using Eq. (20) with sign $\left(\lambda_h(\widetilde{t}_0)\right) = 1$. Let I be the trajectory point where $\boldsymbol{a} \cdot \hat{\boldsymbol{i}}_\theta$ reverses its sign. This point is reached at $\widetilde{t}_I$ and is placed at a distance $\widetilde{r}_I$ from the primary. Figures 3(a)–3(c) show that $\widetilde{t}_I$ decreases as $\widetilde{a}_T$ is increased, which implies a reduction of the range within which $\widetilde{h}' > 0$.

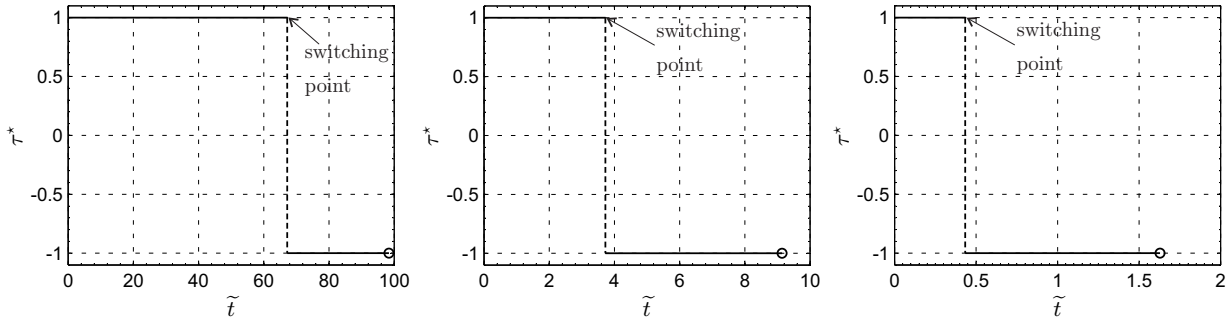

(a) $\widetilde{a}_T = 0.01$. (b) $\widetilde{a}_T = 0.1$. (c) $\widetilde{a}_T = 1$.

Figure 3: Optimal control law $\tau^\star = \tau^\star(\widetilde{t})$ as a function of $\widetilde{a}_T = \{0.01, 0.1, 1\}$.

Figure 4 illustrates the time histories of the adjoint functions, which are necessary for reproducing the optimal transfer trajectories of Fig. 5. Note that these functions are rather involved, with a number of local minima, especially for small values of $\widetilde{a}_T$. The initial value of λ_h is positive and coincides with the result given by Eq. (20). Table 1 summarizes the main characteristics of the optimal transfer orbits in the three

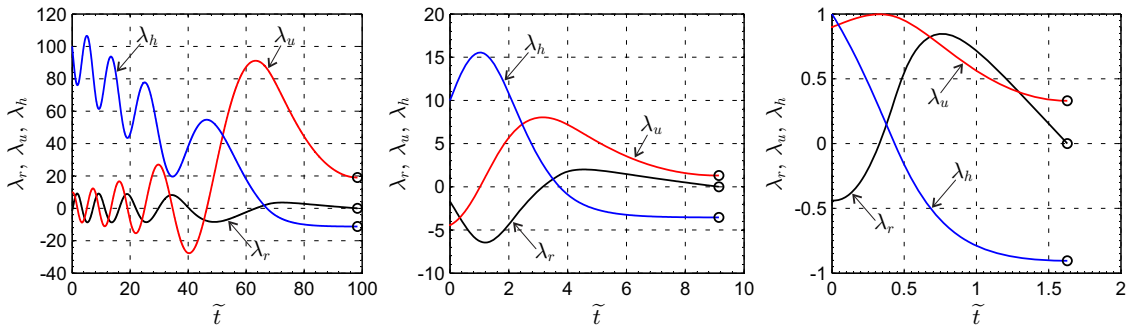

(a) $\widetilde{a}_T = 0.01$. (b) $\widetilde{a}_T = 0.1$. (c) $\widetilde{a}_T = 1$.

Figure 4: Time variation of the dimensionless adjoint functions $\{\lambda_r, \lambda_u, \lambda_h\}$ along the optimal trajectory as a function of $\widetilde{a}_T = \{0.01, 0.1, 1\}$.

exemplary cases. The final value of the polar angle is θ_f, which coincides with the angular position of point A.

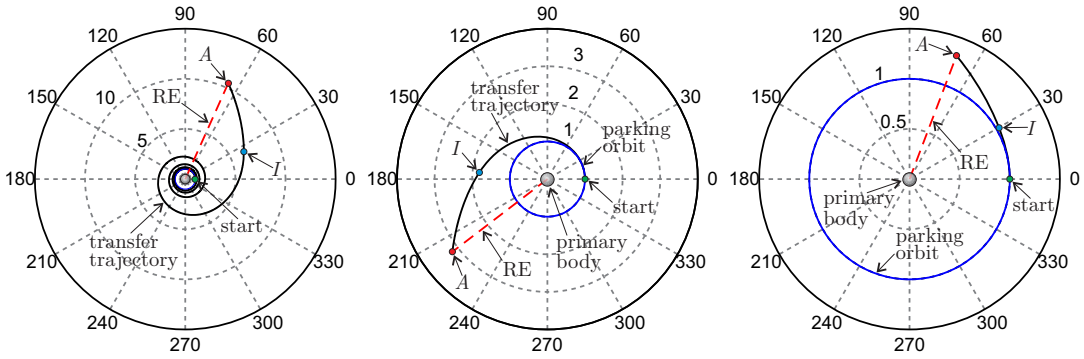

(a) $\widetilde{a}_T = 0.01$. (b) $\widetilde{a}_T = 0.1$. (c) $\widetilde{a}_T = 1$.

Figure 5: Polar form of the optimal transfer trajectory as a function of $\widetilde{a}_T = \{0.01, 0.1, 1\}$.

	$\widetilde{a}_T$		
	0.01	0.1	1
$\widetilde{t}_f$	98.4112	9.1439	1.6287
$\theta_f/(2\pi)$	4.1828	0.6039	0.1921
$\widetilde{r}_A$	10.4821	3.1826	1.3167
$\widetilde{t}_I$	67.1991	3.7243	0.4335
$\widetilde{r}_I$	6.4443	1.8166	1.0293
$\lambda_r(\widetilde{t}_0)$	−1.6069	−1.6972	−0.4388
$\lambda_u(\widetilde{t}_0)$	9.6719	−4.4515	0.8986
$\lambda_h(\widetilde{t}_0)$	100	10	1

Table 1: Optimal transfer orbit characteristics as a function of $\widetilde{a}_T = \{0.01, 0.1, 1\}$.

3.1. Parametric analysis

The optimal trajectories of the three exemplary cases are useful for a parametric study of the minimum time transfers in which the propulsive acceleration is varied within the range $\widetilde{a}_T \in [0.01, 1]$ with a step size of $\Delta\widetilde{a}_T = 1/2000$. In fact, the TPBVP associated to the optimal problem has been analyzed starting from an acceleration level $\widetilde{a}_T = 1$ and decreasing such value, for each problem to address, of an amount equal to the step size. In doing so, the i-th problem, characterized by a propulsive acceleration $\widetilde{a}_T = 1 - i\,\Delta\widetilde{a}_T$, has been solved by taking the adjoint variables obtained from the previous $(i-1)$-th problem as their initial guesses. The solution of the whole set of optimal transfer trajectories allows the curve describing the minimum time variation as a function of the maximum propulsive acceleration magnitude to be found numerically. Such a result is shown in Fig. 6, where the distance $\widetilde{r}_A$ from the primary and the final polar angle θ_f are also reported.

The variations of $\{\widetilde{t}_f, \widetilde{r}_A, \theta_f\}$ with $\widetilde{a}_T \in [0.01, 1]$ may also be interpolated (with a few tenths percent error) through the following functions

$$\widetilde{t}_f \simeq \frac{0.9856}{\widetilde{a}_T} \tag{21}$$

$$\widetilde{r}_A \simeq \frac{1.14\,\widetilde{a}_T + 0.2647}{\widetilde{a}_T + 0.01807} \tag{22}$$

$$\frac{\theta_f}{2\,\pi} \simeq 0.1896 + \frac{0.04039}{\widetilde{a}_T} \tag{23}$$

For a given value of $\widetilde{a}_T$, the optimal control law is univocally defined by the switching time $\widetilde{t}_I$ and the corresponding distance from the primary $\widetilde{r}_I$, which are graphically obtained from Fig. 7, or analytically approximated by the relations

$$\widetilde{t}_I \simeq \frac{0.5778}{\widetilde{a}_T} \tag{24}$$

$$\widetilde{r}_I \simeq \frac{0.8579\,\widetilde{a}_T + 0.1195}{\widetilde{a}_T + 0.00971} \tag{25}$$

Note that Eqs. (21)–(25) are consistent with the results of numerical simulations (with a few tenths percent error only) provided the dimensionless propulsive acceleration magnitude ranges in the interval

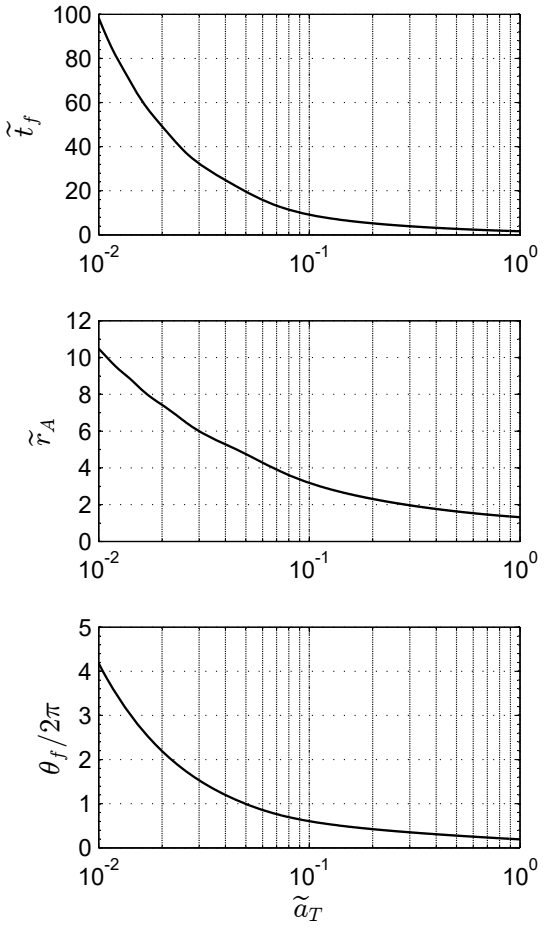

Figure 6: Minimum flight time, apocenter radius, and final polar angle as a function of $\widetilde{a}_T \in [0.01,\, 1]$.

$\widetilde{a}_T \in [0.01,\, 1]$. The initial values of the three adjoint variables $\{\lambda_r,\, \lambda_u,\, \lambda_h\}$ are useful for simulating the optimal control law. For that reason Fig. 8 summarizes the results obtained from numerical simulations. In particular, the curve describing $\lambda_h(\widetilde{t}_0)$ as a function of $\widetilde{a}_T$ is in agreement with Eq. (20).

It is interesting to compare the minimum time solutions using a propulsion system with a continuous circumferential thrust with those achievable using a multi-impulse approach, in order to quantify the differences in terms of transfer performance in the two cases. This subject is discussed in the next section.

3.2. Multi-impulse transfer scenario

The continuous thrust case, investigated in the previous sections, is now approximated by a number of impulsive manoeuvres, and the optimal trajectory (in terms of minimum total transfer time) is calculated for comparative purposes using such a different approach. The optimal solution in this case is obtained using the Sims-Flanagan transcription method [20] with some additional assumptions. In particular, the whole spacecraft trajectory is divided into intervals of equal time length $\Delta\widetilde{t}_{\rm int}$ with

$$\Delta\widetilde{t}_{\rm int} = \frac{\widetilde{t}_f}{N-1} \tag{26}$$

where N is the total number of impulsive manoeuvres.

The continuous thrust acting on the spacecraft during each time interval is approximated by an impulsive manoeuvre applied in the middle of the interval. Each velocity change $\Delta\widetilde{\boldsymbol{v}}_i$ is assumed to take place along the circumferential direction and is therefore written as

$$\Delta\widetilde{\boldsymbol{v}}_i = \tau_i\, \widetilde{a}_T\, \Delta\widetilde{t}_{\rm int}\, \hat{\boldsymbol{i}}_\theta \qquad \text{with} \qquad i = 1, .., N \tag{27}$$

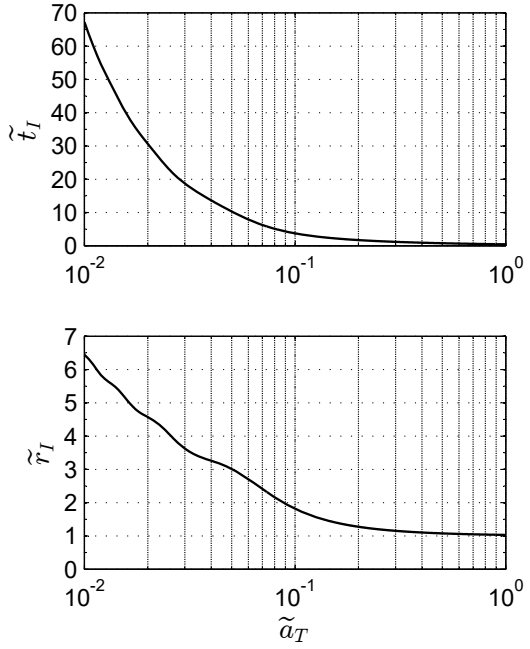

Figure 7: Switching radius and time as a function of $\widetilde{a}_T \in [0.01,\ 1]$.

where $\tau_i \in [-1, 1]$. A two-body model is used to propagate each trajectory leg between two succeeding impulses, so that the whole trajectory is fully obtained by solving $N-1$ Kepler's problems. The problem is to minimize the total flight time $\widetilde{t}_f$ using $\{\tau_1, \tau_2, \ldots, \tau_N\}$ as the set of control variables, while enforcing the final spacecraft velocity to be zero. Note that the total number of impulses represents a tradeoff parameter between computational cost and capability of better approximating the continuous thrust case.

Global optimization algorithms have been used to find the optimal trajectory, which was then refined through a non-linear programming problem solver [20]. The minimum transfer time required to reach the apocenter of an ERO has been calculated in the three previous exemplary cases characterized by $\widetilde{a}_T = \{0.01,\ 0.1,\ 1\}$, assuming a circular parking orbit of radius $\widetilde{r}(\widetilde{t}_0) = 1$. For example, when the number of impulses is $N = 50$, the optimal transfer orbit characteristics are summarized in Table 2. As expected, a

	$\widetilde{a}_T$		
	0.01	0.1	1
$\widetilde{t}_f$	97.0249	8.9501	1.5933
$\theta_f/(2\pi)$	4.0935	0.5887	0.1889
$\widetilde{r}_A$	10.2371	3.1506	1.3085
$\widetilde{t}_I$	67.3234	3.6531	0.4227
$\widetilde{r}_I$	6.4185	1.8252	1.0305

Table 2: Optimal multi-impulse transfer orbit characteristics as a function of $\widetilde{a}_T = \{0.01,\ 0.1,\ 1\}$ when $N = 50$.

comparison between Table 2 and Table 1 shows that the differences between the results obtained with a continuous thrust and a multi-impulse strategy tend to increase as the acceleration level $\widetilde{a}_T$ is decreased. However, the simplified method described in this section is shown to be very efficient in finding a good approximation of the optimal continuous thrust solution (at least for high values of the propulsive acceleration

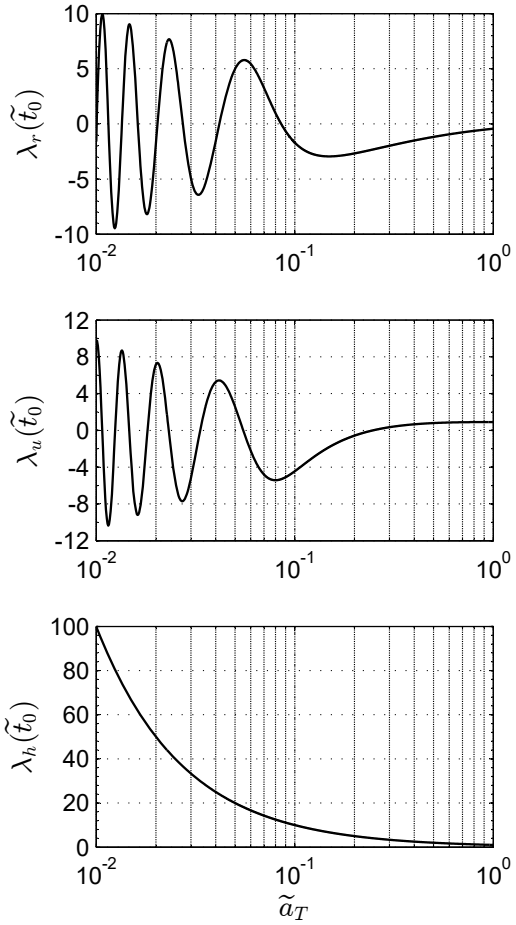

Figure 8: Initial value of adjoint dimensionless variables as a function of $\widetilde{a}_T \in [0.01, 1]$.

magnitude). Note that, unlike the indirect approach, this method does not require any initial guess of the optimal solution, since the optimization algorithm generates a random initial population of feasible solutions.

3.2.1. Minimization of total velocity variation

In this section the optimization of the transfer trajectory toward the apocenter of an ERO is investigated considering the total velocity change $\Delta\boldsymbol{v}_{\rm tot}$ as the performance index to minimize, while the total flight time t_f may vary within a given time interval. In this case, the control variables are the components of each velocity variation $\Delta\boldsymbol{v}_i$ (whose direction is now left unconstrained) and the flight times along each trajectory leg between two succeeding impulses.

Taking into account that the spacecraft initial conditions (position $\boldsymbol{r}_0$ and velocity $\boldsymbol{v}_0$) are given, the total velocity change can be evaluated as a function of the number N of impulses, as is now described. First, the spacecraft velocity at the beginning of the first trajectory leg is obtained as $\boldsymbol{v}_s^{(1)} = \boldsymbol{v}_0 + \Delta\boldsymbol{v}_0$, where $\Delta\boldsymbol{v}_0$ is the velocity variation at the first impulsive manoeuvre. Then, the position and the velocity just before the application of the succeeding manoeuvre can be computed by solving a Kepler's problem, once the flight time along the trajectory leg is known. The velocity at the beginning of the succeeding leg is simply the sum of the latter velocity and the velocity change associated to the next impulsive manoeuvre. This procedure is repeated for each impulsive manoeuvre, that is

$$\boldsymbol{v}_s^{(i+1)} = \boldsymbol{v}_e^{(i)} + \Delta\boldsymbol{v}_i \qquad \text{with} \qquad i = 1, .., N-2 \tag{28}$$

where $\boldsymbol{v}_e^{(i)}$ is the spacecraft velocity at the end of the i-th leg, and $\boldsymbol{v}_s^{(i+1)}$ is the velocity at the beginning of the $(i+1)$-th leg, see Fig. 9. The total velocity variation $\Delta\boldsymbol{v}_{\rm tot}$ is therefore

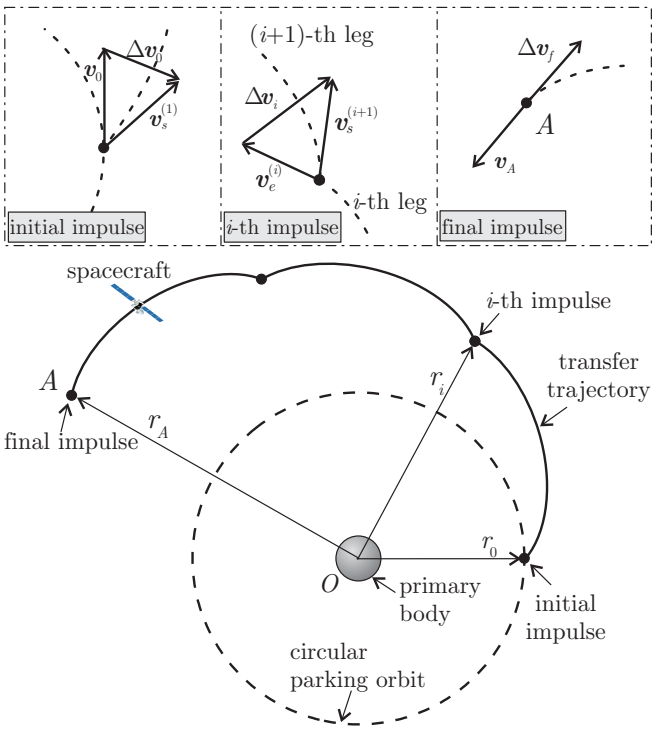

Figure 9: Conceptual sketch of the multi-impulse transfer.

$$\Delta \boldsymbol{v}_{\rm tot} = \Delta \boldsymbol{v}_0 + \sum_{i=1}^{N-2} \Delta \boldsymbol{v}_i + \Delta \boldsymbol{v}_f \tag{29}$$

Note that the last impulsive manoeuvre $\Delta \boldsymbol{v}_f$ is not a control variable, but is obtained by enforcing the final spacecraft velocity to be zero, viz.

$$\Delta \boldsymbol{v}_f = -\boldsymbol{v}_A \tag{30}$$

where $\boldsymbol{v}_A$ is the spacecraft velocity when it reaches the apocenter A of the ERO.

The optimization problem was solved with a global optimization algorithm based on the use of both genetic algorithms and differential evolution methods. When the number N of impulsive maneuvers is given, and assuming that each velocity variation does not exceed a maximum allowable magnitude, the optimal control law is found to consist of one or more impulses concentrated at the initial time (which may be though of as equivalent to a single impulsive manoeuvre), and a final impulse that allows the spacecraft to be put into the ERO. These initial velocity variation vectors are tangent to the circular parking orbit, whereas the magnitude of all other intermediate impulses is equal to zero. As a result, the optimal transfer orbit resembles a Hohmann-like trajectory (see Fig. 10), and the required total velocity change can be written as a function of $\widetilde{r}_A$ as [11]

$$\Delta \widetilde{v}_{\rm tot} = \sqrt{2 - \frac{2}{1+\widetilde{r}_A}} - 1 + \sqrt{\frac{1}{\widetilde{r}_A}} \sqrt{2 - \frac{2\widetilde{r}_A}{1+\widetilde{r}_A}} \tag{31}$$

where $\Delta \widetilde{v}_{\rm tot} = \Delta v_{\rm tot} / \sqrt{\mu / r_0}$, while the dimensionless total time of flight is

$$\Delta \widetilde{t} = \pi \sqrt{\frac{(1+\widetilde{r}_A)^3}{8}} \tag{32}$$

The variation of $\Delta \widetilde{v}_{\rm tot}$ and $\Delta \widetilde{t}$ with $\widetilde{r}_A$ is reported in Fig. 11. In particular, Fig. 11 shows that the higher the apocenter radius, the lower (higher) is the required velocity change (flight time). However, Fig. 11 (or

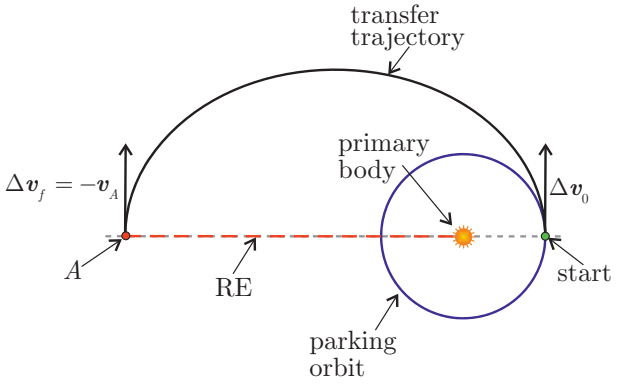

Figure 10: Conceptual sketch of a Hohmann-like transfer trajectory toward the apocenter of a rectilinear ellipse.

Eq. (31)) clearly shows that a multi-impulse transfer towards the apocenter of a ERO requires a high value of the total velocity change.

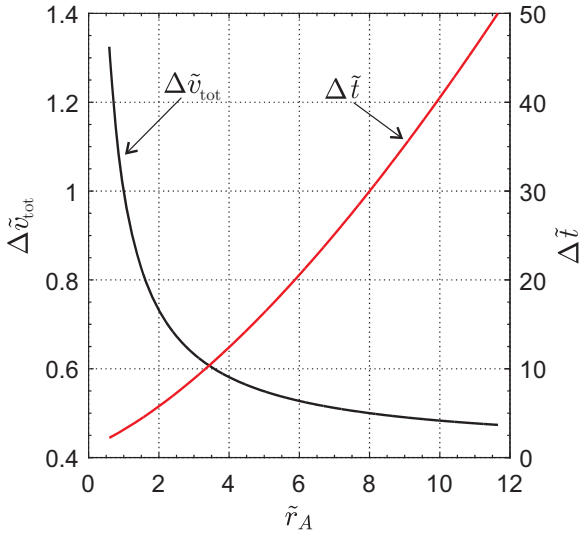

Figure 11: Total velocity change and flight time as a function of $\tilde{r}_A$ in a multi-impulse transfer scenario.

4. Case study

The curves of Figs. 6-7, or their mathematical approximations given by Eqs. (21)–(25), are useful for a preliminary mission analysis, as they relate the ERO geometry with the propulsive acceleration magnitude. For exemplary purposes consider a heliocentric mission scenario ($\mu = \mu_\odot = 132\,712\,439\,935\,\text{km}^3/\text{s}^2$) in which the spacecraft reaches an ERO with aphelion distance $r_A = 5\,\text{au}$ starting from a circular orbit of radius $r(t_0) = 1\,\text{au}$. Once the aphelion A is reached, the spacecraft starts a rectilinear trajectory towards the Sun that coincides with the scientific mission phase [12, 10, 11]. A high value of the aphelion distance allows the flight time along the ERO to be sufficiently long [10] before the spacecraft reaches a critical (small) distance from the Sun, which causes the probe destruction. Therefore, r_A affects the scientific phase of the mission in terms of time interval available for observations and data measurements. For example, when $r_A = 5\,\text{au}$, the scientific phase length necessary to reach the critical distance from the Sun of 0.1 au is about two years [10].

According to Eq. (22), the optimal circumferential propulsive acceleration required for the spacecraft to reach an ERO with $\widetilde{r}_A = 5$ is about $a_T \simeq 0.27\,\mathrm{mm/s^2}$, the flight time is $t_f \simeq 1268\,\mathrm{days} \simeq 3.5\,\mathrm{years}$, whereas the propulsive acceleration reverses its direction at time $t_I \simeq 744\,\mathrm{days}$, when the spacecraft is at a distance $r_I \simeq 3\,\mathrm{au}$ from the Sun, see Eqs. (21) and (24)-(25). In this case, the optimal spacecraft transfer trajectory is shown in Fig. 12, and the time variations of r, u and v are shown in Fig. 13.

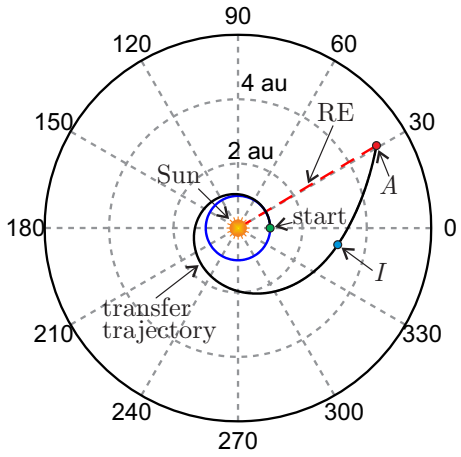

Figure 12: Polar form of the optimal transfer trajectory when $r_A = 5\,\mathrm{au}$ and $a_T = 0.27\,\mathrm{mm/s^2}$.

In particular, the function $v = v(t)$ has a discontinuity in the first derivative when the thrust direction is inverted. Note that using a multi-impulse scenario, an ERO with the same apocenter radius would require a flight time of about 950 days (less than that necessary with a continuous acceleration), at the expense of a very high velocity change, that is, $\Delta v_{\mathrm{tot}} = 16.36\,\mathrm{km/s}$, see Eq. (31).

5. Conclusions

Optimal missions toward the apocenter of rectilinear ellipses have been studied with an indirect approach considering a spacecraft propelled by a circumferential acceleration. The problem solution requires the use of adjoint variables, whose initial values are given by means of suitable graphs that may be used for reproducing the optimal control law. The numerical results have been used to obtain, through an interpolation procedure, a set of analytical expressions that give the optimal transfer characteristics as functions of the propulsive acceleration magnitude. These approximated functions are useful for a preliminary analysis with low computational effort. The performance of the continuous propulsive acceleration case has been compared with that obtained by considering an optimal, multi-impulse transfer scenario, revealing the latter to require a very high value of the total velocity variation.

A possible extension of this work is to analyze the transfer trajectories that minimize the propulsive acceleration magnitude necessary to reach a prescribed rectilinear ellipse in a given flight time. The results of this new problem, combined with the approximate equations discussed in this paper, may be successfully used to get a thorough parametric analysis of the optimal transfer toward a rectilinear orbit with a circumferential propulsive acceleration of constant magnitude.

References

[1] H. S. Tsien, Take-off from satellite orbit, Journal of the American Rocket Society 23 (4) (1953) 233–236, doi: 10.2514/8.4599.

[2] R. H. Battin, An Introduction to the Mathematics and Methods of Astrodynamics, Revised Edition, AIAA, Reston, Virginia, 1999, Ch. 10, pp. 408–418, ISBN: 1-56347-342-9.

[3] A. E. Petropoulos, J. A. Sims, A review of some exact solutions to the planar equations of motion of a thrusting spacecraft, in: 2nd International Symposium on Low-Thrust Trajectory (LoTus-2), Toulouse, France, 2002.

[4] L. Niccolai, A. A. Quarta, G. Mengali, Orbital motion approximation with constant circumferential acceleration, In press. Journal of Guidance, Control, and Dynamics .

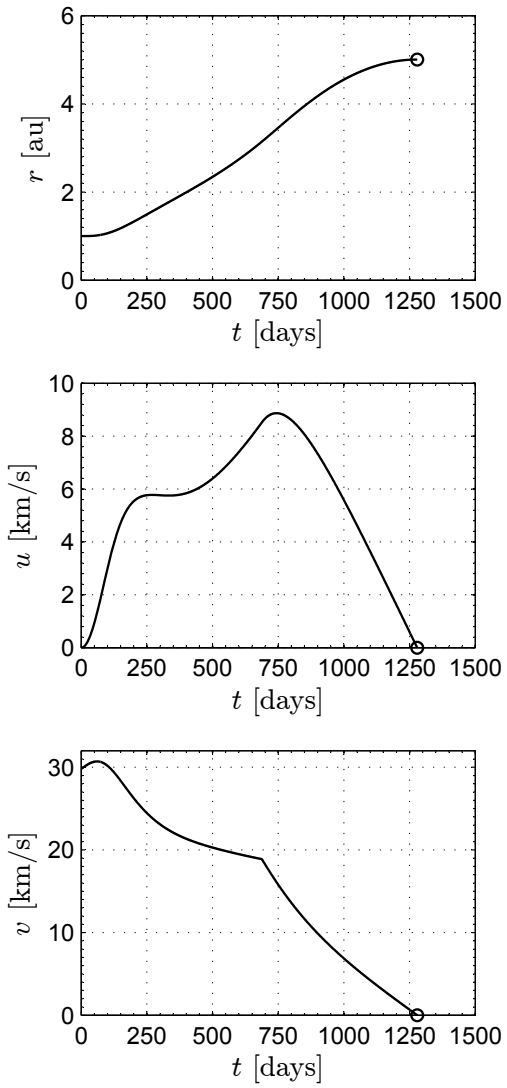

Figure 13: Time variation of the spacecraft state on the optimal transfer trajectory when $r_A = 5\,\text{au}$.

[5] C. Bombardelli, G. Baú, J. Peláez, Asymptotic solution for the two-body problem with constant tangential thrust acceleration, Celestial Mechanics and Dynamical Astronomy 110 (3) (2011) 239–256, doi: 10.1007/s10569-011-9353-3.

[6] A. A. Quarta, G. Mengali, Analysis of spacecraft motion under constant circumferential propulsive acceleration, Acta Astronautica 105 (1) (2014) 278–284, doi: 10.1016/j.actaastro.2014.09.018.

[7] A. E. Roy, Orbital Motion, 4th Edition, Advances in Design and Control, Institute of Physics Publishing, Bristol, UK, 2005, pp. 87–89, ISBN: 0750310154.

[8] I. Dandouras, B. Pirard, J. Y. Prado, High performance solar sails for linear trajectories and heliostationary missions, Advances in Space Research 34 (1) (2004) 198–203, doi: 10.1016/j.asr.2003.02.055.

[9] G. Mengali, A. A. Quarta, Optimal heliostationary missions of high-performance sailcraft, Acta Astronautica 60 (8-9) (2007) 676–683, doi: 10.1016/j.actaastro.2006.07.018.

[10] A. A. Quarta, G. Mengali, Solar sail capabilities to reach elliptic rectilinear orbits, Journal of Guidance, Control, and Dynamics 34 (3) (2011) 923–926, doi: 10.2514/1.51638.

[11] A. A. Quarta, G. Mengali, Optimal solar sail transfer to linear trajectories, Acta Astronautica 82 (2) (2013) 189–196, doi: 10.1016/j.actaastro.2012.03.005.

[12] G. Colombo, D. A. Lautman, G. Pettengill, An alternative option to the dual-probe out-of-ecliptic mission via Jupiter swingby, in: Proc. of the Symp. on the Study of the Sun and Interplanetary Medium in Three Dimensions, no. N76-24119 14-92, NASA GSFC, 1976, pp. 37–47.

[13] G. Mengali, A. A. Quarta, D. Romagnoli, C. Circi, H2-reversal trajectory: a new mission application for high-performance solar sails, Advances in Space Research 48 (11) (2011) 1763–1777, doi: 10.1016/j.asr.2010.11.037.

[14] X. Y. Zeng, H. Baoyin, J. F. Li, S. P. Gong, New applications of the h-reversal trajectory using solar sails, Research in Astronomy and Astrophysics 11 (7) (2011) 863–878, doi: 10.1088/1674-4527/11/7/011.
[15] A. E. Bryson, Y. C. Ho, Applied Optimal Control, Hemisphere Publishing Corporation, New York, NY, 1975, Ch. 2, pp. 71–89, ISBN: 0-891-16228-3.
[16] R. F. Stengel, Optimal Control and Estimation, Dover Publications, inc., 1994, pp. 222–254.
[17] G. Mengali, A. A. Quarta, Optimal three-dimensional interplanetary rendezvous using nonideal solar sail, Journal of Guidance, Control, and Dynamics 28 (1) (2005) 173–177, doi: 10.2514/1.8325.
[18] L. F. Shampine, M. K. Gordon, Computer Solution of Ordinary Differential Equations: The Initial Value Problem, W. H. Freeman, San Francisco, 1975, Ch. 10.
[19] L. F. Shampine, M. W. Reichelt, The matlab ode suite, SIAM Journal on Scientific Computing 18 (1) (1997) 1–22 .
[20] J. A. Sims, S. N. Flanagan, Preliminary design of low-thrust interplanetary missions, in: AAS/AIAA Astrodynamics Specialist Conference, Girdwood, Alaska , 1999, AAS Paper 99-338.

Author biography

Alessandro A. Quarta received his Ph.D. degree in Aerospace Engineering from the University of Pisa in 2005, and is currently Professor of Flight Mechanics at the Department of Civil and Industrial Engineering of the University of Pisa. His main research areas include spaceflight simulation, spacecraft mission analysis and design, low-thrust trajectory optimization, solar sail and E-sail dynamics and control. E-mail: a.quarta@ing.unipi.it.

Giovanni Mengali received the Doctor Engineer degree in Aeronautical Engineering in 1989 from the University of Pisa. Since 1990 he has been with the Department of Aerospace Engineering (now Department of Civil and Industrial Engineering) of the University of Pisa, first as a PhD student, then as an Assistant and an Associate Professor. Currently, he is Professor of Space Flight Mechanics. His main research areas include spacecraft mission analysis, trajectory optimization, solar sails, electric sails and aircraft flight dynamics and control. E-mail: g.mengali@ing.unipi.it.

Andrea Caruso received his B.S. and M.S. degrees in Aerospace Engineering from University of Pisa in 2013 and 2016. He is currently a Ph.D. student at the University of Pisa. His research interests are in spaceflight mechanics and spacecraft trajectory optimization. E-mail: andrea.caruso@ing.unipi.it.